

©1999 American Physical Society

Lipatov, A. S., and G. P. Zank. "Pickup Ion Acceleration at Low- β p Perpendicular Shocks." *Physical Review Letters* 82, no. 18 (May 3, 1999): 3609–12. <https://doi.org/10.1103/PhysRevLett.82.3609>.

Access to this work was provided by the University of Maryland, Baltimore County (UMBC) ScholarWorks@UMBC digital repository on the Maryland Shared Open Access (MD-SOAR) platform.

Please provide feedback

Please support the ScholarWorks@UMBC repository by emailing scholarworks-group@umbc.edu and telling us what having access to this work means to you and why it's important to you. Thank you.

Pickup Ion Acceleration at Low- β_p Perpendicular Shocks

A. S. Lipatov^{1,2,3,*} and G. P. Zank^{1,†}

¹*Bartol Research Institute, University of Delaware, Newark, Delaware 19716*

²*Department of Problems of Physics and Energetics, Moscow Institute of Physics and Technology,
Profsovnaznaia Street 84/32, 117810 Moscow, Russia*

³*Dialogue-Science Inc., Computer Center Russian Academy of Science, Vavilova Street 40, 117333 Moscow, Russia*
(Received 27 July 1998; revised manuscript received 17 December 1998)

Multiscale hybrid kinetic simulations of low- β_p supercritical shocks demonstrate that pickup ions may be strongly accelerated by shock surfing, also known as multiply reflected ion acceleration.
[S0031-9007(99)09039-0]

PACS numbers: 52.35.Tc, 52.65.Rr, 96.50.Fm

In this Letter, we present multiscale hybrid kinetic simulations of low- β_p ($\beta_p \leq 0.1$) supercritical perpendicular shocks (LBSPSs) which demonstrate that these shocks can significantly accelerate pickup ions (PIs) from an initial thermal shell distribution to large energies. This work offers some resolution to the long-standing theoretical puzzle of how some thermal ion subpopulation acquires sufficient energy to be diffusively accelerated at a perpendicular shock wave. Accordingly, the results presented here have immediate and important implications for the acceleration of ions in astrophysical environments as diverse as supernovae shocks, cometary shocks, interplanetary shocks, and stellar wind termination shocks. The simulations demonstrate self-consistently for the first time a new and fundamental dissipation mechanism for quasiperpendicular shocks, and one with the implication that perpendicular shocks can be very efficient in accelerating ions. A hybrid electromagnetic particle-mesh code (which includes the electron inertia term) is employed to simulate LBSPSs with a low PI density in one spatial dimension. The code allows for the analysis of the microscale proton and PI dynamics inside the foot and ramp of the shock transition layer.

The simulations were motivated by the direct observation of accelerated pickup ions near comets and planetary bow shocks, at interplanetary shocks, and by the expectation that the termination shock might be responsible for the acceleration of anomalous cosmic rays. Accelerated pickup ions have been observed directly, for example, by Ulysses at a weak corotating shock [1]. Both pickup H^+ and He^+ were observed by the SWICS instrument to possess very hard power law spectra which extend directly out of the expected pickup ion distribution [2], to energies well in excess of the characteristic pickup ion cutoff velocity $v = 2u_{SW}$ (in the spacecraft frame), where v denotes particle velocity and u_{SW} the solar wind flow velocity. It was observed too that $\sim 43\%$ of the pickup protons H^+ and $\sim 16\%$ of the He^+ was accelerated by the shock. The hardness of the pickup ion spectrum was quite inconsistent with the expectations of diffusive/first-order Fermi shock acceleration. Second, it is generally thought that diffusive shock acceleration should favor the acceleration

of heavy ions over lighter ions since the larger gyroradii ions would be “injected” more easily into the acceleration process. That neither expectation is met poses a challenge for models of particle acceleration at shock waves. Finally, particle acceleration processes are important too in the context of laboratory shocks and shocks generated by active experiments in space.

Besides diffusive shock acceleration, two alternatives for accelerating pickup ions at weak quasiperpendicular shocks are shock drift acceleration [3] and multiply reflected ion (MRI) acceleration or shock surfing, proposed originally in [4], and later in the context of pickup ion acceleration in [5,6]. Both approaches directly accelerate particles out of the pickup ion “thermal” pool. However, the MRI mechanism is found to produce high energies for pickup ions and a very flat spectrum and to have an injection efficiency which decreases with increasing particle mass. Present models of MRI acceleration are either purely analytic [6] or quasianalytic [5], test-particle tracing [7] or test particle-mesh simulations [8], and treat the pickup ions as test particles and use non-self-consistent electromagnetic fields.

Unfortunately, self-consistent kinetic simulations of quasiperpendicular shocks (e.g., [9–12], which may include PIs [13,14]), have yet to demonstrate any significant acceleration of solar wind protons and PIs by MRI-like processes in the absence of either strong wave generation or externally imposed high levels of MHD turbulence.

The basic idea of particle acceleration by the multiple reflection (or surfing) of PIs at the shock ramp is easily explained. On the PI shell distribution in the shock frame, a fraction of the PI population has so little kinetic energy that they can be reflected by the shock electrostatic potential jump inside the ramp, illustrated in Fig. 1 of [5]. This population of ions then drifts along the shock front surface, being multiply reflected at the shock ramp, trapped by the upstream particle Lorentz force and the electrostatic potential jump. The time spent upstream of the shock determines the maximum energy gain for a trapped PI, resulting from a balance between the particle Lorentz force and the gradient of the electrostatic potential.

We now present simulations of LBSPs that exhibit significant MRI energization of PIs at the shock ramp. The simulation results were obtained by using a one-dimensional, $(1 + 2/2)$ D hybrid kinetic electromagnetic code [for ions and protons, we use a kinetic/particle description while for finite mass electrons, the hydrodynamical equations (electron pressure equation) are used] [15]. Anomalous resistivity and electron inertia terms are included in this code. The results in this paper are one dimensional, as we assume spatial variation along the z direction only, but retain all three components of the electromagnetic fields and particle velocities. The shocks studied have upstream parameters, which are expected of the solar wind in the transition layer of the termination shock: $M_A = 3-5$, $\beta_e = 0.1-2.0$, $\beta_p = 0.1-1.0$, $n_{PI}/n_0 = 0.001-0.1$, $M/m = 10^2-10^4$, $M_{PI}/M = 1$, $\omega_{pi}/\omega_{ci} = 4 \times 10^3$, $DZ = 10r_{ci}$, $\Delta_z = (0.006-0.0125)c/\omega_{pi}$, $\theta_{BN} = 90^\circ, 72^\circ$, and $l_d = (0.001-0.25)c/\omega_{pi}$, where M_A is the Alfvén Mach number, $\beta_{p(e)}$ denotes the solar wind proton (electron) plasma beta, n_{PI}/n_0 is the ratio of PI to proton density, M/m is the ratio of proton to electron mass, M_{PI}/M is the ratio of PI to proton mass, DZ is the size of the simulation box, Δ_z is the cell size, $r_{ci} = u_0/\Omega_i$ is the proton cyclotron radius ($r_{ci} = r_{cH^+}$), and $l_d = \nu c^2/\omega_{pi}^2 u_0$ is the resistive diffusion length [9,11], where ν is the anomalous collision frequency.

The chosen range of the resistive diffusion length corresponds to current-driven instabilities in the foot and ramp: for the ion acoustic mode, $\nu_{IA} \approx 10^{-2}\omega_{pe}$, $l_{d,IA} \approx 0.2c/\omega_{pi}$; for the lower-hybrid drift mode, $\nu_{LH} \approx 2.2 \times$

$10^{-4}\omega_{pe}$, $l_{d,LH} \approx 3.8 \times 10^{-3}c/\omega_{pi}$, and for the modified two-stream instability, $\nu_{MTS} \approx 2.2 \times 10^{-5}\omega_{pe}$, $l_{d,MTS} \approx 3.8 \times 10^{-4}c/\omega_{pi}$. These scales are consistent with observational and theoretical studies of instabilities at shock fronts [16]. Initially, the proton velocity distribution function is Maxwellian, with a PI shell velocity distribution in velocity space, which we assume to have been thickened. The interior shell radius is taken to be $V_{int} = 1.1u_0$ and that of the exterior shell is $V_{ext} = 1.5u_0$, where u_0 denotes upstream bulk velocity. Note that the effective upstream bulk velocity relative to the shock front (in the simulation) is $1.4u_0$ and the effective interior and exterior shell radii are 0.8 and 1.07, respectively. This is not a very sensitive assumption. The bulk velocity of PIs equals the bulk velocity of protons at the initial moment of time $\mathbf{u}_{PI} = \mathbf{u}_0$. There are 4097–8193 cells in z , and initially 512 000 macroprotons and 512 000 macroions. Plasma is injected continuously into the left of the simulation box and the shock is formed by reflecting the plasma off the right-hand end of the box. The simulation time step is $5 \times 10^{-5}T_{ci}$, where $T_{ci} = 2\pi/\Omega_i$ and Ω_i is the proton gyrofrequency. Such small spatial and time scales were chosen to resolve the ramp on an electron inertial length scale and to provide an accurate calculation of PI trajectories as they are transmitted across the ramp.

Figure 1 illustrates a simulation of a shock with $M_A = 5$, $n_{PI}/n_0 = 0.01$, and $l_d = 0.006c/\omega_{pi}$ at time $t = 3.8T_{ci}$. Note that we show only half the simulation box. In the figure, the velocity, magnetic field, density, and electron pressure are normalized to the upstream velocity, magnetic field, proton density, and electron pressure.

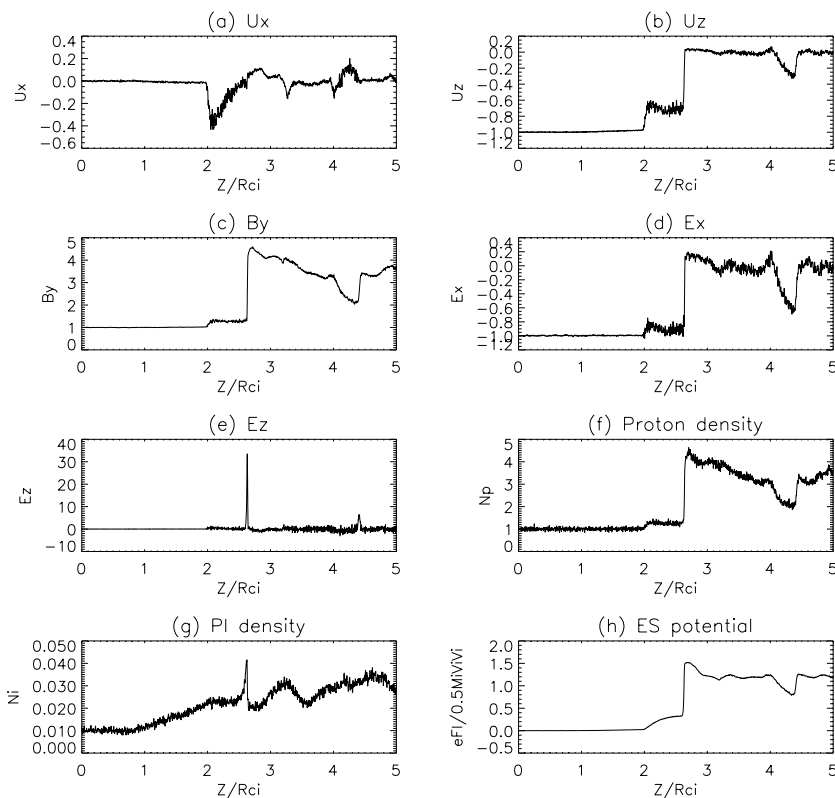


FIG. 1. Typical profiles of the bulk velocity components u_x and u_z , the magnetic field component B_y , the electric components E_x and E_z , the proton n_p and PI n_{PI} densities, and electrostatic potential $e\phi/Mu_0^2/2$.

The electric field and electrostatic potential are normalized to the upstream motional electric field $u_0 B_0/c$ and the kinetic energy of incoming protons $Mu_0^2/2$. The simulation demonstrates the formation of a shock transition layer with a strong foot in the PI density profile (g) and a thin ramp, $\Delta_{\text{ramp}}/r_{ci} < 0.05$ in the magnetic field and electrostatic potential profiles, Figs. 1c and 1h. An additional jump forms at a distance $\delta z \approx 0.6r_{ci}$ before the ramp in the electromagnetic field, bulk velocity, and proton density profiles. It is clearly seen that the peak in PI density corresponds to accelerated PIs and the peak is located inside the shock ramp due to temporary trapping of PIs, Fig. 1g.

Figure 2 shows $v_{\perp 2}$ vs $v_{\perp 1}$ for the protons and H^+ PIs at different locations relative to the shock ramp. The panels of Fig. 2 are arranged in ascending order from the bottom according to position as follows: far upstream (bottom panel), on the shock front, just downstream of the shock, and the top panel, far downstream. The left (right) column illustrates the projected proton (PI) distribution in the plane ($v_{\perp 1}, v_{\perp 2}$) at various distances from the shock ramp, where $v_{\perp 1}$ and $v_{\perp 2}$ are the velocity components, perpendicular to the magnetic field. The proton distribution function has a supersonic core ahead of the ramp and a subsonic core downstream of the shock front. Before the ramp, we see reflected protons, while downstream the transmitted protons form a halo due to phase mixing. The bottom right panel illustrates a very typical distribution which results from ion reflection at a perpendicular shock. Such distributions are seen at virtually all quasiperpendicular shocks, both observationally (e.g., [17]) and in simulations (e.g., [9]), and contribute essentially to the formation of the ion shock foot. If the number and energy density of the reflected PIs were sufficiently high at the termination shock, the foot structure and length scales would be determined primarily by reflected PIs rather than the colder more numerous solar wind protons [5,14]. The second panel from the bottom shows the PI distribution at the shock ramp and a strong transverse acceleration of PIs along the shock front is evident with the formation of an extended “tongue” along $v_{\perp 2}$. Finally, phase mixing occurs far downstream.

Figure 3 illustrates the energy spectrum of accelerated H^+ PIs for spatial sections ranging from downstream to upstream. The PI energy spectrum has two parts, as discussed by [5]; a shell-like distribution with an energy cutoff at about $E_0 = M_{PI}u_0^2/2$ in the solar wind frame and an accelerated PI component which emerges from the shell distribution as a hard/flat power law spectrum. The accelerated PI energy spectrum may be approximated by the power law $F_i \propto dN/N \sim (E/E_0)^{-k}$, where the energy E is calculated in the solar wind frame and N denotes the PI number density. In the present case, the index k is about 1.0–1.3 in the vicinity of the ramp. The similarity between the spectra produced by the hybrid simulation here, a test particle-mesh simulation [8], and those obtained from the quasianalytical approach of [5] is close. The spectrum produced by the

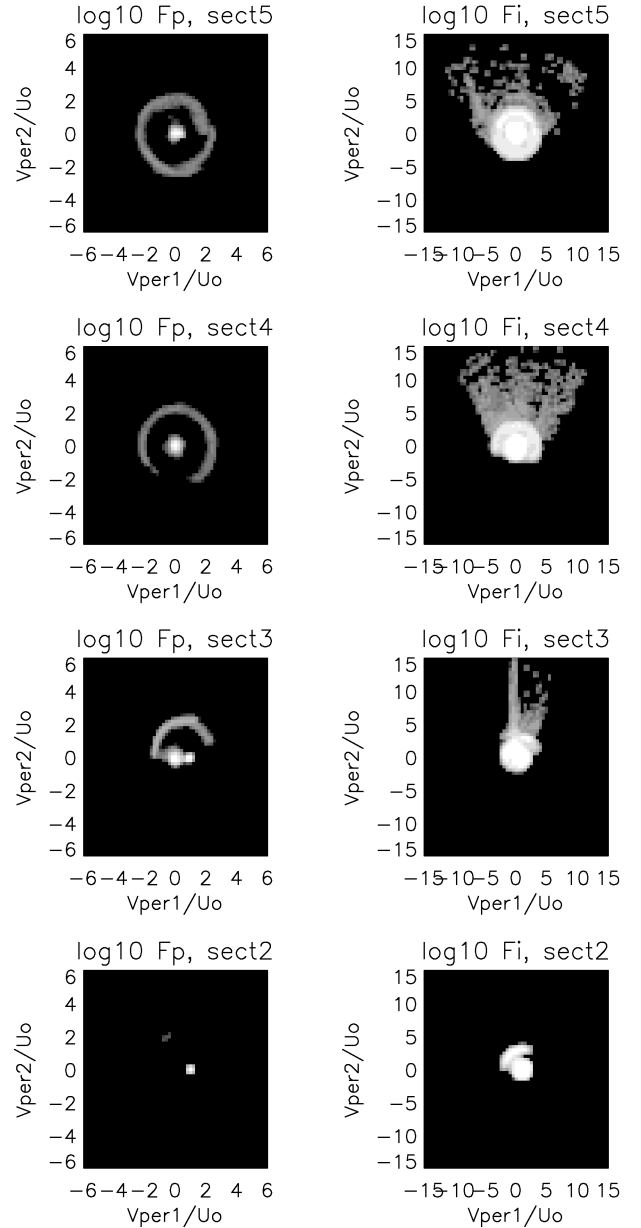


FIG. 2. The projection of the protons (left column) and H^+ PI (right column) distribution onto the velocity plane for spatial sections ranging from downstream to upstream. Here $v_{\perp 1} \parallel \mathbf{v}_z$ and $v_{\perp 2} \parallel \mathbf{v}_x$ are the velocity components perpendicular to the magnetic field.

MRI mechanism is much harder than expected of diffusive shock acceleration, which would produce an E^{-2} spectrum for the shock compression ratio used in our test-particle simulations. Also, as discussed in §2 of [5], diffusive shock acceleration at a perpendicular shock imposes severe energy constraints on the particles to be accelerated, constraints which are absent for MRI acceleration. The maximum transverse energy of accelerated PIs ($\log_{10} E_{\text{max}}/E_0 = 2.3-2.5$) is higher than estimated by [5] for a ramp thickness is about $L_{\text{ramp}} < 0.05r_{ci}$. The simulation with a high PI density ($n_{PI}/n_0 = 0.1$) is less efficient at accelerating PIs ($\log_{10} E_{\text{max}}/E_0 = 1.7$) thanks

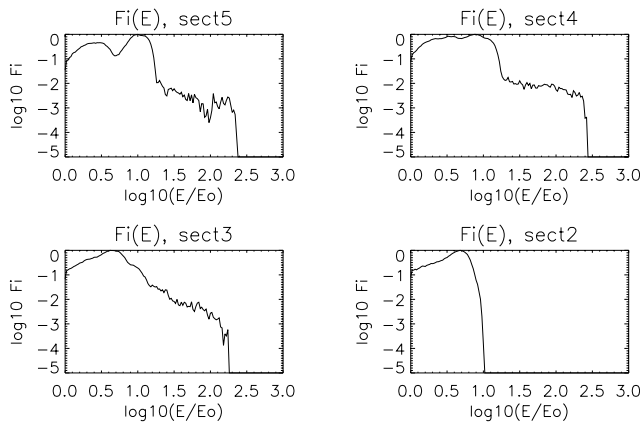


FIG. 3. The energy spectrum of accelerated H^+ PIs for spatial sections ranging from downstream to upstream.

to the formation of a strong foot and a decrease in the electrostatic potential jump. In the simulation with large resistive diffusion length $l_d = 0.25c/\omega_{pi}$, the maximum energy of accelerated PIs significantly decreases since the ramp thickness is too large, and MRI acceleration becomes ineffective. For the simulation with small resistive diffusion length, $l_d = 0.001c/\omega_{pi}$, the electrostatic jump at the ramp is comparable with the fluctuation level and no significant acceleration occurs. In the quasiperpendicular case, $\theta_{BN} = 72^\circ$, the formation of a whistler precursor decreases the efficacy of PI acceleration.

In conclusion, kinetic hybrid simulations of the acceleration of H^+ pickup ions at low- $\beta_p \leq 0.1$ collisionless quasiperpendicular shocks [with a low PI density ($n_{PI}/n_0 < 0.1$) and appropriate anomalous resistivity $0.006c/\omega_{pi} \leq l_d < 0.25c/\omega_{pi}$] have demonstrated several new features, as well as providing support for the basic test-particle analysis of Refs. [5–8]. Our results may be enumerated as follows. (1) The energy spectrum of accelerated H^+ PIs at quasiperpendicular shocks may be approximated by the power law $F_i(E) \approx (E/E_0)^{-k}$, where k varies from 1.0 to 1.3. This spectrum is a little harder than that obtained by the quasianalytical approach of Ref. [5] but both approaches give spectra which are considerably harder than those predicted by diffusive shock acceleration. (2) For MRI acceleration of H^+ and He^+ ions to be effective, a ramp thickness comparable to the electron inertial length scale is needed, whereas for heavy ions, it is sufficient to have a ramp thickness comparable to that of the ion inertial length. Thus, the key factor determining the efficacy of MRI acceleration is the existence of a strong steep ramp inside the shock transition layer. The simulation does not show MRI acceleration of H^+ and He^+ at shocks with $\beta_p > 0.1$.

G.P.Z. and A.S.L. were supported in part by an NSF-DOE Grant No. ATM 9713223, NASA Grant No. NAG5-6469, an NSF Young Investigator Award No. ATM-9357861, JPL Contract No. 959167, NASA Delaware Space Grant No. NGT5-40024, and Russian Science Foundation Grant No. 96-02-16326. A.S.L.

thanks K. Papadopoulos and R.Z. Sagdeev for fruitful discussions about our simulation model.

*Email address: lipat@dials.ccas.ru

†Email address: zank@bartol.udel.edu

- [1] G. Gloeckler *et al.*, J. Geophys. Res. **99**, 17 637 (1994).
- [2] V.M. Vasyliunas and G.L. Siscoe, J. Geophys. Res. **81**, 1247 (1976).
- [3] R.B. Decker, Space Sci. Rev. **48**, 195 (1988); T.P. Armstrong, M.E. Pesses, and R.B. Decker, in *Collisionless Shocks in the Heliosphere: Reviews of Current Research*, Geophysical Monograph Series, Vol. 35, edited by B.T. Tsurutani and R.G. Stone (American Geophysical Union, Washington, DC, 1985), p. 271; R.B. Decker and L. Vlahos, Astrophys. J. **306**, 710 (1986).
- [4] R.Z. Sagdeev, in *Reviews of Plasma Physics*, edited by M.A. Leontovich (Consultants Bureau, New York, 1966), Vol. 4, p. 23; R.Z. Sagdeev and V.D. Shapiro, Sov. JETP Lett. **17**, 279 (1973); T. Katsouleas and J.M. Dawson, Phys. Rev. Lett. **51**, 392 (1983).
- [5] G.P. Zank, H.L. Pauls, I.H. Cairns, and G.M. Webb, J. Geophys. Res. **101**, 457 (1996).
- [6] M.A. Lee, V.D. Shapiro, and R.Z. Sagdeev, J. Geophys. Res. **101**, 4777 (1996).
- [7] D. Zilbersher and M. Gedalin, Planet. Space Sci. **45**, 693 (1997).
- [8] A.S. Lipatov, G.P. Zank, and H.L. Pauls, J. Geophys. Res. **103**, 29 679 (1998).
- [9] M.A. Leroy *et al.*, J. Geophys. Res. **87**, 5081 (1982).
- [10] K.B. Quest, Phys. Rev. Lett. **54**, 1872 (1985).
- [11] K.B. Quest, J. Geophys. Res. **91**, 8805 (1986).
- [12] D.W. Forslund, K.B. Quest, J.U. Brackbill, and K. Lee, J. Geophys. Res. **89**, 2142 (1984); R.L. Tokar, C.H. Aldrich, D.W. Forslund, and K.B. Quest, Phys. Rev. Lett. **56**, 1909 (1986); B. Lembege and J.M. Dawson, Phys. Rev. Lett. **62**, 2683 (1989); A.S. Lipatov and V.A. Lobachev, Cosm. Res. **34**, 420 (1996).
- [13] A.A. Galeev, A.S. Lipatov, and R.Z. Sagdeev, Sov. Phys. JETP **62**, 866 (1985); A.S. Lipatov and I.N. Syrovatskii, Cosm. Res. **25**, 750 (1987); N. Omidi and D. Winske, J. Geophys. Res. **92**, 13 409 (1987); P.C. Liewer, S. Rath, and B.E. Goldstein, J. Geophys. Res. **100**, 19 809 (1995); J. Giacalone, J.R. Jokipii, and J. Kóta, J. Geophys. Res. **99**, 19 351 (1994); H. Kucharek and M. Scholer, J. Geophys. Res. **100**, 1745 (1995).
- [14] P.C. Liewer, B.E. Goldstein, and N. Omidi, J. Geophys. Res. **98**, 15 211 (1993).
- [15] A.A. Galeev, A.S. Lipatov, and A.A. Malgichev, Sov. J. Plasma Phys. **17**, 701 (1991); A.S. Lipatov, Cosm. Res. **32**, 72 (1994).
- [16] J.D. Scudder *et al.*, J. Geophys. Res. **91**, 11 019 (1986); K. Papadopoulos, in *Collisionless Shocks in the Heliosphere: A Tutorial Review*, Geophysical Monograph Series, Vol. 34, edited by R.G. Stone and B.T. Tsurutani (American Geophysical Union, Washington, DC, 1985), pp. 59–90; C.F. Kennel, J.P. Edmiston, and T. Hada, *ibid.*, pp. 1–36; D. Winske, in *Collisionless Shocks in the Heliosphere: Reviews of Current Research* (Ref. [3]), p. 225.
- [17] N. Sckopke, Adv. Space Res. **15**, 261 (1995).